Chemical Engineering Journal 388 (2020) 124237

Contents lists available at ScienceDirect

Chemical Engineering Journal

journal homepage: www.elsevier.com/locate/cej

Platinum nanoparticle-assembled porous biogenic silica 3D hybrid structures with outstanding 4-nitrophenol degradation performance

Naveen Kumar Reddy Bogireddy[a], Padma Sahare[b], Umapada Pal[c], Sion Federico Olive Méndez[d], Lorenzo Martinez Gomez[e], Vivechana Agarwal[a,*]

[a] Centro de Investigación en Ingeniería y Ciencias Aplicadas, UAEM, Av. Univ. 1001, Col. Chamilpa, Cuernavaca, Morelos 62209, Mexico
[b] Instituto de Física y Matemáticas, Universidad Michoacana de San Nicolás de Hidalgo, Morelia, Michoacán, Mexico
[c] Instituto de Física, Benemérita Universidad Autónoma de Puebla, Apdo. Postal J-48, Puebla 72570, Mexico
[d] Centro de Investigación en Materiales Avanzados, S.C. (CIMAV), Miguel de Cervantes No. 120, C.P. 31136 Chihuahua, Chih., Mexico
[e] Universidad Nacional Autónoma de México, Instituto de Ciencias Físicas, Av. Universidad s/n, Cuernavaca, MOR 62210, Mexico

HIGHLIGHTS

- Small PtNPs assembled over 3D biogenic porous silica from 3 different origins.
- Porous hybrid revealed outstanding catalytic performance in 4-nitrophenol reduction.
- High stability without significant change in catalytic efficiency after 8 cycles.
- Short purification time in 4-NP spiked water for possible industrial applications.
- PtSiOx catalyst may act as in-built depth filter to trap the suspended contaminants.

GRAPHICAL ABSTRACT

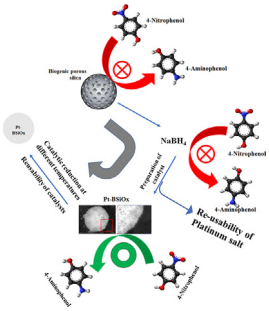

ARTICLE INFO

Keywords:
Platinum nanoparticles
Biogenic silica
Hybrid structures
Degradation of 4-nitrophenol
Catalysis

ABSTRACT

Pt/biogenic SiO_2 hybrid structures were fabricated by assembling Pt nanoparticles over biogenic porous silica particles from three different sources. Apart from analyzing their morphology, composition and microstructure, the catalytic activity of the nanocomposites have been tested for the degradation of 4-nitrophenol, which is one of the most frequent contaminants in waste water emanation from pharmaceutical and textile industries. The Pt/SiO_2 hybrid structures derived from *Equisetum myriohaetum* (EM) porous silica revealed a complete reduction of 4-NP (to 4-AP) within 90 s at room temperature, and within 20 s at 70 °C. The catalytic activity and apparent kinetic rate constants (k_{app}, $111 \times 10^{-3}\ s^{-1}$ at 70 °C) of the Pt/SiO_2 catalyst were found to be much superior to the corresponding parameters of Ag or Au nanoparticles supported over silica and other common semiconducting supports. The high turnover capacity of the porous silica supported catalyst (7.59 min^{-1} at 70 °C) could be associated to the presence of ample active sites in densely assembled Pt particles over 3D silica surface, which facilitates the electron transfer process from Pt particles to adsorbed 4-NP molecules. Excellent reusability (only 3% decrease after 8 cycles) of the hybrid catalyst for the purification of 4-NP polluted water in "filtering and catalyzing" device has been demonstrated.

* Corresponding author.
E-mail address: vagarwal@uaem.mx (V. Agarwal).

https://doi.org/10.1016/j.cej.2020.124237
Received 1 October 2019; Received in revised form 22 December 2019; Accepted 26 January 2020
Available online 28 January 2020

Nomenclature

EM/EMB	*Equisetum myriohaetum*
BB	bamboo
RH	Rice husk
SiOx	silica
TOC	turnover capacity
4-NP	4-nitrophenol
4-AP	4-aminophenol
PtNPs	Platinum nanoparticles
C	Carbon
AgNPs	silver nanoparticle
AuNPs	gold nanoparticles
RT	room temperature
APTES	(3-Aminopropyl) triethoxysilane

1. Introduction

Over the past few decades, accidental release of oil and organic solvents during their extraction, transportation, and storage have resulted in a detrimental impact on marine and land ecology. In order to address this issue, various adsorbent materials such as, crosslinked polymers and resins [1], polymer gels [2], nanocomposites [3], fibers [4], organic-inorganic hybrids [5], carbon-based materials [6] and silica [7] have been developed. However, most of them suffer from low adsorption capacity for organic solvents. Moreover, due to powdered texture, they are difficult to separate and hence have poor reusability. Although microporous polymers with large specific surface area are known for high adsorption capacity, they are relatively expensive, and their environmental risks are still unclear [8]. On the other hand, noble metal nanoparticles (NMNPs), especially platinum nanoparticles (PtNPs) have shown great promise as heterogeneous catalysts for the degradation/reduction of the organic pollutants [9,10].

While Pt NPs of smaller sizes manifest higher catalytic activity, [11] due to bigger surface area and high surface energy, they tend to aggregate, which reduces their organic pollutant reduction efficiency significantly [12]. On the other hand, these NPs of very small size are difficult to separate from catalytic reaction solutions. To overcome those limitations, frequently the NMNPs are assembled over the surface of solid substrates (e.g., organic polymers, metal oxides, clays, zeolites, and carbons) [13]. Substantial efforts have also been made for designing assembled NMNPs over silica supports for their catalytic use [14].

In this respect, use of biogenic silica particles has several advantages. First, biogenic silica particles have high surface area with micro-, meso- and macro-pores which can facilitate the diffusion and transport of organic pollutant molecules and ions. Second, their integrated morphology not only offers effective pollutant reduction with reusability option, but also helps to minimize potential environmental risks caused by accidental release (leaching) of support materials, which frequently lead the production of toxic by-products, causing environmental pollution [13]. Third, these 3D structures are highly stable, which can work in a wide temperature range [15] and harsh acidic conditions [16]. In addition, biogenic silica can act as in-built depth filter, where the suspended contaminants can be trapped within the depth of the porous catalytic system.

On the other hand, 4-nitrophenol (4-NP) is one of the most popular organic compounds used in the production of pesticides, which is carcinogenic and genotoxic to humans and animals [17]. Furthermore, 4-Aminophenol (4-AP) is an important industrial intermediate applied in the production of analgesic/ antipyretic drugs and for corrosion inhibition. The reduction of 4-NP over NMNPs in the presence of $NaBH_4$ is a well-known eco-friendly probe reaction to produce 4-AP [18–20]. However, most of the recently reported catalysts [18,20] demonstrate low degradation efficiency and turnover capacities in the reduction of 4-NP. In addition, the catalysts remain in water and are harmful to the organisms in the ecosystem. In order to solve these problems, filtration and separation process are required to remove the suspending solids and contaminants from liquid. Use of mesoporous support such as biogenic silica may facilitate in-depth filtration of the suspended contaminants (smaller than the pore volume) [20].

Here we present the fabrication of small (≈2.2 nm average size) Pt nanoparticles, assembled over porous 3D biogenic silica extracted from rice husk, *Equisetum myriohaetum* and bamboo. The simple *in situ* Pt salt reduction within the functionalized porous biogenic silica resulted in the formation and assembly of the Pt NPs onto the supports, to form the hybrid catalysts. Apart from studying the size, morphology, crystallinity, and chemical sate of the Pt NPs, the fabricated nanocomposites have been tested for catalytic degradation of 4-NP in aqueous solution. Observed high catalytic activity of the biogenic silica-supported Pt NPs has been explained through the presence of high density active catalytic sites in them and highly porous nature of the used biogenic silica particles. Catalytic performances of the fabricated nanostructures in the reduction of 4-nitrophenol to 4-aminophenol in presence of $NaBH_4$ have been compared with the performance of other NMNP-supported composite catalysts.

2. Experimental section

2.1. Materials

For the present work, rice husk and *Equisetum myriohaetum* (Mexican Giant Horsetail) were obtained from Morelos state, Mexico, while commercial biogenic porous silica (*Concretio silicea bambuseae* or "Bamboo") was acquired from Bristol Botanicals Ltd, UK. Hexachloroplatinic acid (H_2PtCl_6, 8 wt% in H_2O), 4-nitrophenol (4-NP, spectrophotometric grade), sodium borohydride ($NaBH_4$, 99.99%), concentrated hydrochloric acid (37%, HCl), (3-Aminopropyl) triethoxysilane (APTES) and ammonium hydroxide (28%) were purchased from Sigma-Aldrich, and utilized as received.

2.1.1. Synthesis of biogenic porous silica from Equisetum myriohaetum and rice husk

The synthesis procedure and characteristics of 3D biogenic silica extracted from *Equisetum myriohaetum* (Mexican Giant Horsetail) have been discussed in our earlier published article [21]. In brief, the stems of the plant (*Equisetum myriohaetum)* were separated and oven dried at 50 °C prior to acid digestion in concentrated HNO_3/H_2SO_4 (4:1), where 25 g of dry starting material was processed with 1 L of acid. The mixture was stirred and left in a fume hood until a white precipitate was obtained and the release of nitrogen oxides is ceased (usually around 48 h). The precipitate was then separated and washed with copious amounts of deionized water until the pH value of supernatant reaches around 5. The sample was then lyophilized before heat-treatment in air at 650 °C for 5 h, at the heating rate of 10 °C/min. The same protocol was followed for extracting silica from rice husk. The porous silica particles prepared from *Equisetum myriohaetum* and rice husk were designated as EMSiOx, and RHSiOx, respectively. On the other hand, the commercial biogenic silica extracted from bamboo plant was designated as BBSiOx.

2.1.2. Functionalization of 3D silica substrates with APTES

The BBSiOx, RHSiOx and EMSiOx samples were functionalized with APTES using the method reported by Li et al. [14] with some modification, to obtain amino group capped silica substrates. Typically, 1 mL of APTES and 0.10 g of silica were added into 10 mL of ethanol.

The mixture was stirred at room temperature for 8 h. The resultant APTES-modified 3D silica substrates were separated by centrifugation at 7500 rpm, washed several times by ethanol, and then re-dispersed in 9 mL of DI water.

2.1.3. Growth of Pt NPs onto biogenic silica substrates

About 50 mL of an ethanolic H_2PtCl_6 solution (10 mM) was added to 0.10 g of surface modified BBSiOx, RHSiOx or EMSiOx substrates under vigorous magnetic stirring. Within 30 s, the color of the reaction mixture turned from white to dark yellow, indicating the impregnation of the platinum salt into the pores of biogenic silica particles. After 6 h of magnetic stirring under ambient conditions, the samples were separated from the reaction mixture by centrifugation at 7500 rpm to remove excess $PtCl_6^{2-}$ ions, and then re-dispersed in 1 mL of DI water. About 50 μL of ethanolic $NaBH_4$ (40 mg/mL) solution was added to each of the above dispersions under vigorous stirring to reduce the $PtCl_6^{2-}$ ions and formation of small PtNPs onto the 3D silica substrates. Finally, the PtNPs-incorporated 3D silica substrates were separated by centrifugation at 7500 rpm. The as-synthesized PtNPs-incorporated biogenic EM silica, rice husk silica and bamboo silica substrates were designated as Pt-EMSiOx, Pt-RHSiOx and Pt-BBSiOx, respectively. The whole process, from functionalization of silica substrates to the formation of PtNPs has been depicted in Scheme 1.

2.2. Characterization

X-ray diffraction (XRD) analysis of the powder samples was carried out in a Bruker D8 Advance eco diffractometer, using CuK_α (λ = 1.5406 Å) radiation. The size, morphology, and composition of the hybrid catalysts were studied using Hitachi SU5000 Schottky field-emission scanning electron microscope (FESEM) equipped with energy dispersive spectroscopy (EDS) system. High-resolution transmission electron microscopy (HR-TEM) images were acquired using a JEOL JEM 2200Fs + Cs (aberration corrector) with a single tilt sample holder in scanning TEM (STEM) mode and a bright field detector. The samples for TEM study were prepared by dispersing the colloidal samples over Lacey carbon-coated copper grids. The sample loaded copper grids were subjected to plasma cleaning for 15 s at 3.0 mTorr working pressure, to eliminate contaminants and solvent residues. UV–vis optical absorption spectra of the colloidal 3D silica substrates with and without PtNPs were recorded in a dual beam Perkin-Elmer Lambda 950 spectrophotometer. The same spectrophotometer was utilized for monitoring the reduction of 4-NP by the hybrid catalysts. Texture parameters of the hybrid samples were estimated from their N_2 adsorption–desorption isotherms recorded in a Bell Mini-II sorptometer. Approximately 100 mg of each of the powder samples was degassed at 100 °C overnight prior to their analysis. Specific surface area of the hybrid catalysts was determined by the Brunauer–Emmett–Teller (BET) method using a five-point adsorption isotherm in the relative pressure range of P/P_0 = 0.05/0.3 at 77.35 K. Sample porosity (pore size distribution) was obtained by the Barrett-Joyner-Halenda (BJH) method from the desorption branch of the isotherm.

2.3. Catalytic reduction of 4-nitrophenol (4-NP)

Separate sets of experiments were carried out with 0.24 mg of each catalyst i.e., Pt-BBSiOx, Pt-RHSiOx and Pt-EMSiOx. The measured amount of hybrid catalyst (0.24 mg) was dispersed in 30 mL DI water and mixed with 30 mL of aqueous 4-NP (1.0 mM) to form a mixture solution. Subsequently, 3 mL of a freshly prepared $NaBH_4$ solution (0.1 M) was added to the earlier mixture. The 4-NP degradation process was followed by monitoring the change in the optical absorption spectra of the solution in 314 to 400 nm spectral range. A quartz cuvette of 1 cm × 1 cm × 5 cm dimension was utilized for recording the absorption spectra of the test solutions.

To investigate the reusability of the fabricated hybrid catalysts, the procedure stated above was repeated with the catalysts re-collected after use in the 4-NP reduction. The re-collected catalysts were washed repeatedly by centrifugation using DI water. The amount of catalyst, concentration and volume of 4-NP and $NaBH_4$ solutions used for the recyclability tests were also maintained same. All the catalytic tests were performed at room temperature, without stirring the reaction mixture.

As reference, the reduction of 4-NP was also carried out using pristine 3D biogenic silica substrates without adding $NaBH_4$ solution and over PtNPs-incorporated biogenic silica catalysts without adding $NaBH_4$ solution. It was observed that a complete degradation of 4-NP was not possible in absence either of $NaHB_4$ or of hybrid catalyst. To evaluate the proficiency of 4-NP reduction by $NaBH_4$ catalyzed by these hybrid structures, thermodynamic parameters such as entropy, enthalpy, and Gibbs free energy of the catalytic reaction were estimated from the reaction kinetics of the PtNPs-assembled 3D silica supports at different temperatures.

3. Results and discussion

3.1. Catalyst preparation and characterization

Typical TEM images of the samples presented in Fig. 1 clearly revealed the formation of PtNPs, assembled over 3D silica substrates for all the hybrid samples. As can be noticed, PtNPs of 2.0–2.5 nm size range are assembled over the porous silica substrates. The sizes of the Pt

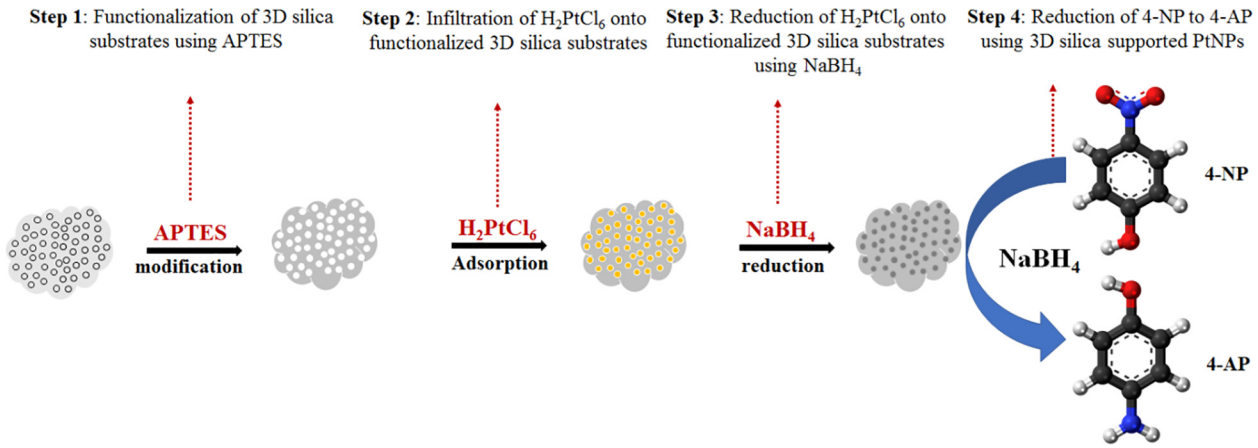

Scheme 1. Schematic representation of the process involved in the preparation of small PtNPs over mesoporous 3D biogenic silica substrates used for the reduction of 4-nitrophenol.

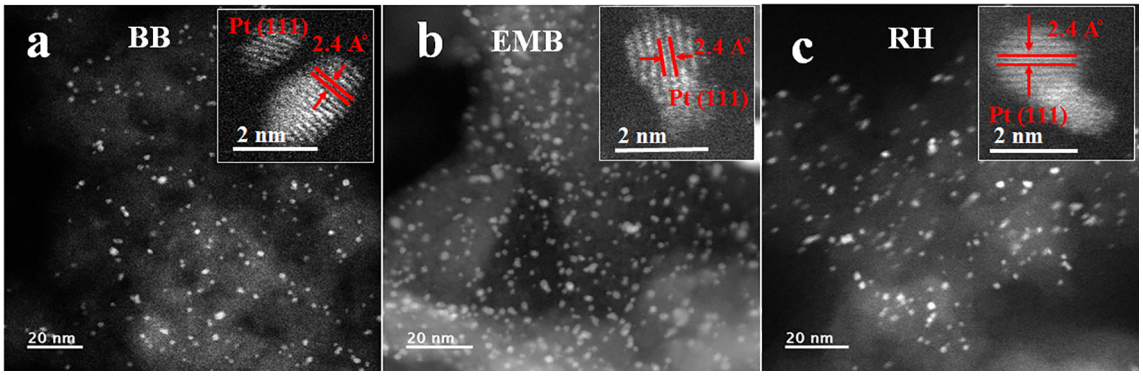

Fig. 1. Typical TEM images of the (a) Pt-BBSiOx, (b) Pt-EMSiOx, and (c) Pt-RHSiOx catalysts, demonstrating the formation of small PtNPs onto 3D biogenic silica substrates. Insets show typical HRTEM images of PtNPs formed over corresponding silica substrates.

NPs are also in good agreement with their grain size values estimated from their XRD patterns. While the reduction of $PtCl_6^{2-}$ ions and the formation of PtNPs over the porous biogenic silica substrates at room temperature are very clear in the TEM micrographs (Fig. 1), highly crystalline nature of the formed PtNPs can be appreciated from the well resolved lattice patterns revealed in their high resolution micrographs presented as insets in Fig. 1. Although the dimensions of the Pt nanoparticles formed over three kinds of porous silica were very similar, the density of PtNPs formed over EM silica (Fig. 1b) is higher than in other two substrates. Typical FESEM and EDS elemental mapping images of the hybrid catalysts presented in Fig. S1 (Supplementary information, SI) clearly revealed the formation of nanometric Pt particles over the sub-micrometric silica particles. Elemental mapping images (Fig. S1, SI) revealed the presence of only silicon (Si) and platinum (Pt) in the hybrid structures.

XRD patterns of the hybrid catalysts were recorded to study the crystallinity of the small PtNPs supported over biogenic silica (Fig. 2 (a-c)). As can be noticed, all the samples revealed a broad diffraction band around 22° corresponding to amorphous silica substrates, apart from several sharp diffraction peaks, characteristic of crystalline platinum particles in face centered cubic (fcc) phase. The diffraction peaks appeared around 40.0, 46.6, 63.14 and 80.34° correspond to the (1 1 1), (2 0 0), (2 2 0) and (3 1 1) lattice planes of metallic platinum in fcc phase (JCPDS # 87–0647) [22]. While the intensity of the diffraction peaks associated to crystalline PtNPs was comparable for the Pt-RHSiOx and Pt-EMSiOx samples, the intensity of the peaks revealed for the Pt-BBSiOx sample was relatively low, probably due to lower Pt content in the sample, compared to other two samples. The average grain sizes of polycrystalline metal particles calculated applying Scherrer formula on the most intense (1 1 1) diffraction peak were about 2.3, 2.5, and 2.4 nm for the Pt-RHSiOx, Pt-BBSiOx and Pt-EMSiOx samples, respectively.

XPS characterization technique was used to obtain information about the oxidation state, relative intensity (counts/s) and atomic % of each of the elements present in the hybrid catalysts. Survey spectra of all the hybrid catalysts (Fig. S2, SI) revealed typical emission bands of O, Si, Pt and C. XPS estimated Pt contents in the Pt-EMSiOx, Pt-RHSiOx, and Pt-BBSiOx hybrid catalysts were 0.82, 0.65, and 0.48 wt%, while the Pt contents estimated through their EDS analysis were 1.65, 1.18, and 1.06 wt%, respectively. The core-level C1s emission bands emanating from Pt-RHSiOx, Pt-EMSiOx and Pt-BBSiOx samples (Fig. 3a) could be de-convoluted into four components peaked around 284.5, 286.0, 287.1 and 288.6 eV, attributed to sp^2 C–C, C–O, C═O and O–C═O bonds, respectively [23].

The O1s emission from SiO_2 is reported to have a binding energy of 533.05 eV [24]. While the binding energy of O1s emission associated to C═O is reported to lie in-between 531.5 and 532.1 eV, its position in the C-OH and/or C-O-C bonds is located in-between 533.6 and 534.1 eV [25]. As can be seen (Fig. 3c), the broad core level O 1s emission of all the samples have four components located around 530.7, 531.6, 532.5, and 533.4 eV. While the component revealed at 530.7 eV can be associated to surface adsorbed hydroxy (OH) groups, the broad component peaked around 532.5 eV fits well with the binding energy of oxygen in SiOx [26]. The position of this component is shifted to lower energy (Fig. 3c) for the Pt-BBSiOx sample. While all the samples revealed a component band around 533.4 eV, associated to C-OH bond, the relative intensity of this band is substantially low for Pt-BBSiOx sample. Lower intensity of this emission for Pt-BBSiOx catalyst might be associated to a lower concentration of PtNPs at BBSiOx surface, anchored with the amino groups of APTES molecules. Finally, the component appeared at binding energy close to 531.6 eV was assigned to the C═O bond formed between the O atoms of SiOx and the organic binder APTES. A higher relative intensity of this component in the Pt-EMSiOx sample is fully commensurated with the higher PtNPs concentration revealed in the corresponding TEM images (Fig. 1b).

The Si $2p_{3/2}$ core-level emissions of the composites could be deconvoluted to 5 components. For the Pt-RHSiOx and Pt-BBSiOx samples, the component bands appeared around binding energies 99.5,

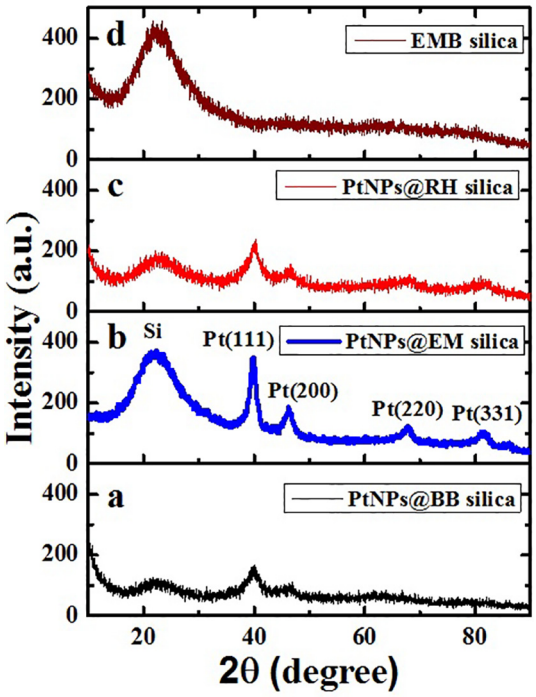

Fig. 2. XRD patterns of PtNPs-incorporated biogenic (a) BB, (b) EM, and (c) RH silica. For reference, XRD pattern of the pristine mesoporous EM silica (control) has been provided in (d).

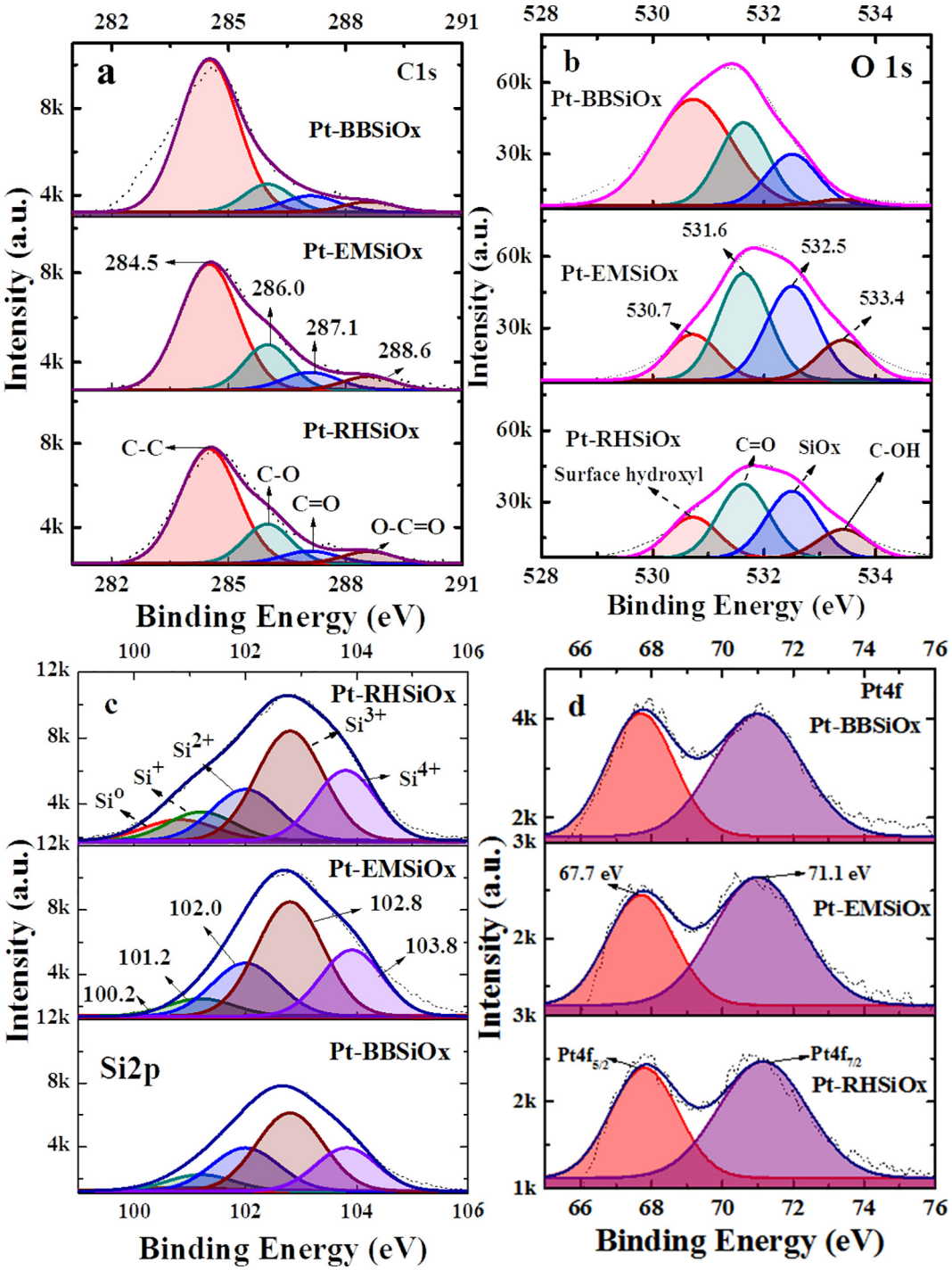

Fig. 3. High-resolution (a) C 1s, (b) O 1s, (c) Si 2p and (d) Pt 4f core-level XPS emissions for the Pt-RHSiOx, Pt-EMSiOx, and Pt-BBSiOx hybrid catalysts.

100.6, 101.5, 102.4 and 103.5 eV. However, for the Pt-EMSiOx sample, the components appeared at about 1.0 eV lower binding energies. The five component emissions could be associated to elemental Si (Si^0), SiO_2 (Si^{+4}), Si_2O (Si^{1+}), SiO (Si^{2+}), and Si_2O_3 (Si^{3+}). [25,26]. As can be noticed, the Si 2p band gets shifted towards lower binding energy with the increase of Pt content (%) in the hybrid catalysts. While the Pt content in the hybrid catalysts varied in the order: Pt-EMSiOx > Pt-RHSiOx> Pt-BBSiOx, the maximum of the Si 2p emission in then varied in the order: 101.2 eV > 102.8 eV > 103.0 eV, respectively. Apart from broadness, such a shift in the position of emission maximum clearly indicates the band consist of different sub-bands with different relative intensities for different samples.

Finally, the core-level Pt 4f emissions of all the samples revealed their Gaussian shaped spin–orbit doublets Pt $4f_{5/2}$ and Pt $4f_{7/2}$ (Fig. 3d) separated by about 3.35 eV, as expected. The binding energy positions of the Pt $4f_{5/2}$ and Pt $4f_{7/2}$ components in the hybrid catalysts vary in-between 67.75 and 67.99 and 71.02–71.21 eV, respectively, which correspond to the metallic Pt(0) [27]. Absence of higher energy (72–76 eV) components, corresponding to Pt(II)/Pt(IV) confirms the complete reduction of Pt salt to Pt (0).

The BET surface area estimation plots, pore size distribution, and texture parameters estimated from the N_2 adsorption-desorption isotherms of the catalysts are presented in Fig. 4. As can be seen, the RHSiOx has slightly higher surface area than EMSiOx catalyst substrate.

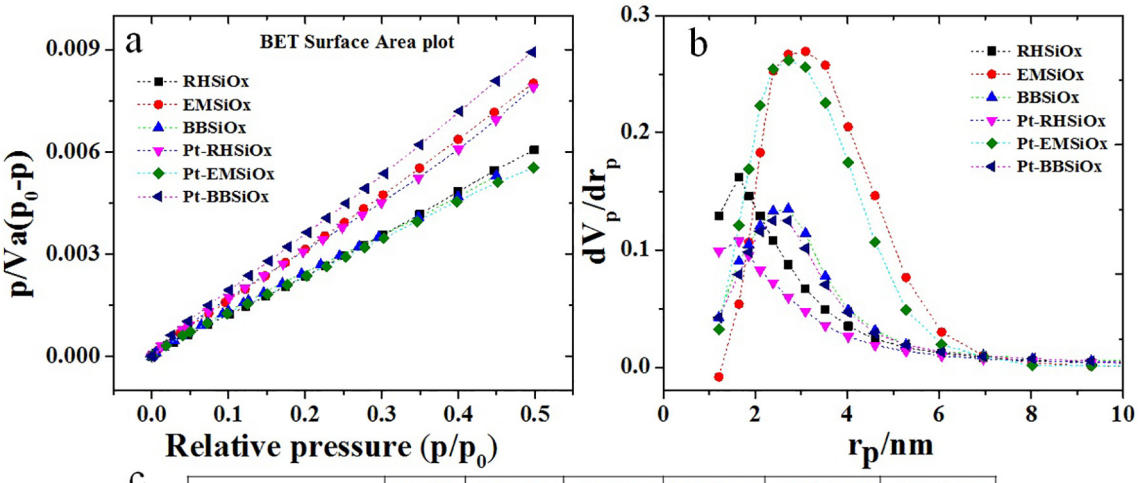

c

	RHSiOx	EMSiOx	BBSiOx	Pt-RHSiOx	Pt-EMSiOx	Pt-BBSiOx
V_m (cm^3g^{-1})	88.735	84.192	63.871	69.288	83.834	57.461
$a_{s,BET}$ (m^2g^{-1})	386.22	364.44	278	301.58	361	250.10
Total pore volumen (p/p_0=0.990) (cm^3g^{-1})	0.4665	0.7656	0.4958	0.3606	0.7263	0.4631
Average pore diameter(nm)	4.8312	8.3571	7.1339	4.7824	7.4303	7.0620

Fig. 4. The texture properties of the biogenic porous SiOx substrates (a) BET surface area analysis, (b) pore size distribution, and (c) texture parameters of all three biogenic SiOx substrates before and after platinum nanoparticle formation onto their surface.

Similarly, the EMSiOx has bigger pores and wider size distribution than the other two substrates. The results indicate the EMSiOx substrate has higher possibility for in-depth filtration, which is an important characteristic of the hybrid substrate for its catalytic applications.

In addition, the room temperature UV–vis absorption spectra of the colloidal biogenic silica particles and the hybrid catalysts are shown in Fig. S3 (SI). The characteristic surface plasmon resonance (SPR) absorption peaks of the silica substrates and PtNPs appeared around 220 and 270 nm, respectively [22].

3.2. Catalytic performance of the hybrid catalysts

The reduction of 4-NP to 4-AP was selected as a probe reaction for testing the catalytic performance of PtNPs assembled over biogenic silica substrates, and the reaction was monitored by UV–vis absorbance spectroscopy. Although the reduction of 4-NP by $NaBH_4$ is feasible thermodynamically due to the positive difference of their standard electrode potentials (ΔE_0 = E_0(4-NP/4-AP) − E_0(H_3BO_3/BH_4) = −0.76 − (−1.33) = 0.67 V), it could be kinetically restricted in the absence of an efficient catalyst [28]. A visual color change from light yellow to bright yellow of the 4-NP solution was observed after the addition of $NaBH_4$ along with a red shift of the absorption peak from 317 to 400 nm (Fig. 5). The ionization of $NaBH_4$ in the aqueous medium followed by the adsorption onto the hybrid catalyst along with the simultaneous adsorption of 4-NP, resulted in the formation of 4-nitrophenolate ions [18–20]. On the other hand, on adding the pristine 3D silica substrates into the reaction solution in absence of $NaBH_4$ solution, no noticeable change in the absorbance of 4-NP ions was observed; which indicates that pure silica substrates do not take part in the 4-NP reduction process (Fig. 5). Fig. 5(c–e) shows the UV–vis absorption spectra during the catalytic reduction of 4-NP in presence of the Pt-BBSiOx catalyst. The strong absorption peak appeared around 400 nm corresponds to 4- nitrophenolate ions, which disappears within 90 s after the addition of the catalyst, generating a new peak at around 300 nm, attributed to 4-AP [20]. Fig. 5 (f-h) further indicates the excellent catalytic property of the PtNPs attached over biogenic silica substrates with a complete reduction of 4-NP within 90 s (Table 1).

Fig. 6 reveals the catalytic reduction of 4-nitrophenol (ratio of 4-NP concentration (evaluated through corresponding absorbance) at time "t" to the initial concentration of 4-NP before adding Pt-BBSiOx hybrid structure as a catalyst vs reduction time (sec)) to 4-aminophenol using Pt-BBSiOx hybrid structure catalyst at 5 different temperatures from 30 °C to 70 °C. From the catalytic reduction analysis of 4-NP, an exponential decay with increasing reduction time (sec) is observed. Pseudo first order ($\ln (C_t/C_0) = -k.t$) equation was applied as relatively higher concentration of $NaBH_4$ was used. Rate constants at each reaction temperature obtained from linear fit of $\ln (C_t/C_0)$ vs time (sec), are found to gradually increase from $12 * 10^{-3}$ s^{-1} to $25 * 10^{-3}$ s^{-1} corresponding to reaction temperatures from 30 °C to 70 °C. These rate constants were used to proceed further to calculate the thermodynamic parameter.

Fig. 7 reveals the catalytic reduction of 4-nitrophenol to 4-aminophenol using Pt-RHSiOx hybrid catalyst as a function of temperature from 30 °C to 70 °C. From the analysis of 4-NP catalytic reduction (following the same procedure used for Pt-BBSiOx hybrid structures), it is clear that there is a gradual increase in the rate constants (k_{app}) from $29 * 10^{-3}$ s^{-1} to $84 * 10^{-3}$ s^{-1} due to the increase of reaction temperatures from 30 °C to 70 °C. The higher k_{app} values for the Pt-RHSiOx hybrid structure as compared to Pt-BBSiOx hybrid structure indicate that the catalytic reduction efficiency of Pt-RHSiOx hybrid structures is superior to the catalytic efficiency of Pt-BBSiOx hybrid structures. Thermodynamic parameters were calculated from these rate constants.

Fig. 8 presents the kinetics of catalytic reduction of 4-nitrophenol to 4-aminophenol by Pt-EMSiOx hybrid catalyst at different temperatures; from 30 °C to 70 °C. From the analysis of 4-NP catalytic reduction (following the same procedure used for Pt-BBSiOx hybrid structures), similar to the above mentioned results from two other Pt based hybrid structures, there is a gradual increase in the rate constants (k_{app}) from $24 * 10^{-3}$ s^{-1} to $111 * 10^{-3}$ s^{-1} with the increase of reaction temperatures from 30 °C to 70 °C. In the present case, greater k_{app} values as compared with Pt-BBSiOx and Pt-RHSiOx hybrid structures is indicative of the higher catalytic reduction efficiency of Pt-EMSiOx hybrid structures with respect to the other hybrid structures (Fig. 9) [19,29–34]. Rate constants were further used to calculate the thermodynamic

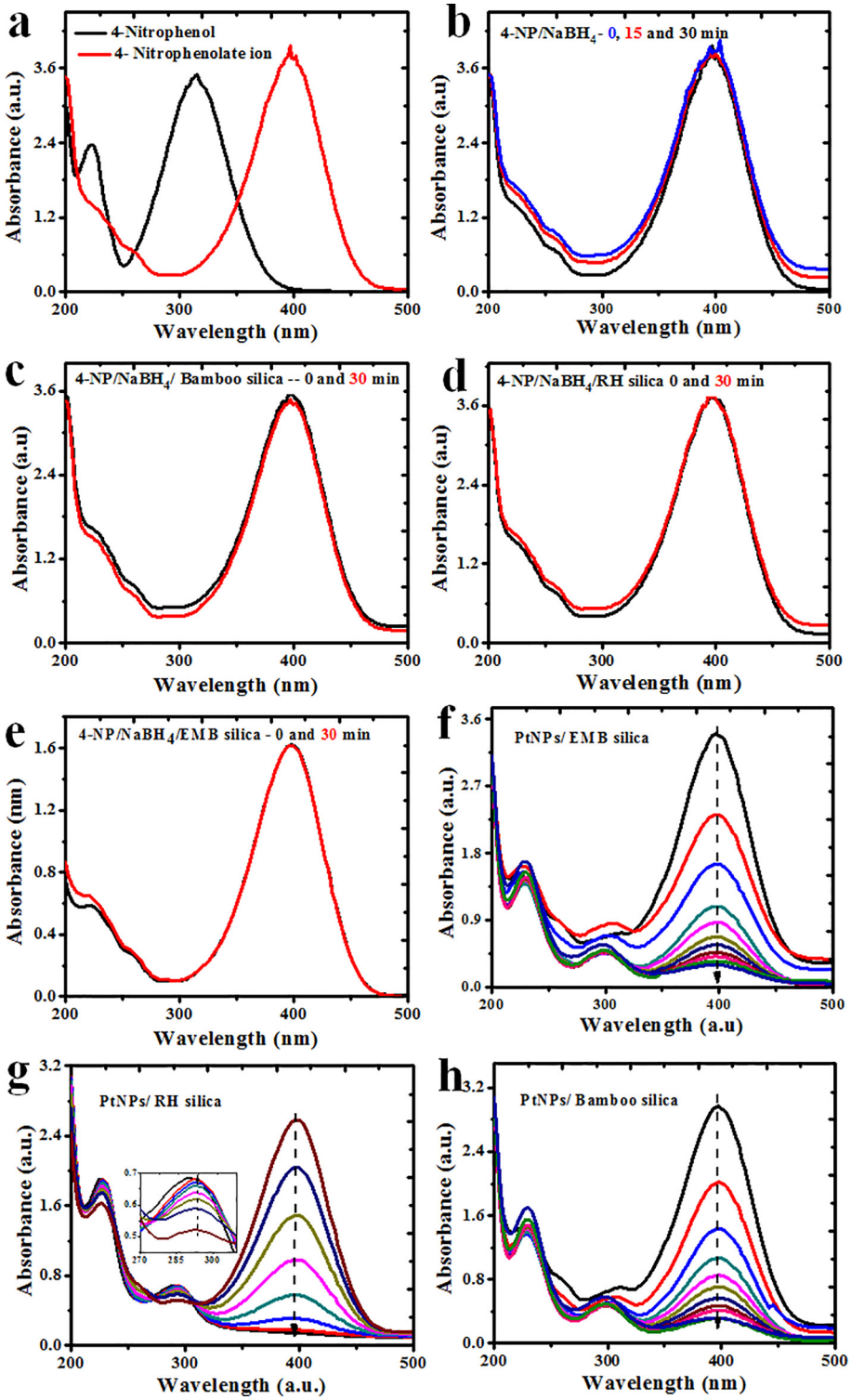

Fig. 5. Absorbance spectra of (a) 4-nitrophenol (4-NP) and 4-nitrophenolate ion before (black) and after (red) the addition of $NaBH_4$ in the solution; (b) 4-NP solution containing $NaBH_4$ (without catalyst) at different time intervals, showing only the absorption band of 4-nitrophenolate ions; $NaBH_4$ containing 4-NP solution after the addition of (c) RH (d) Bamboo, and (e) EM silica. Evolution of absorption spectra after the addition of (f) Pt-EMSiOx, (g) Pt-RHSiOx and (h) Pt-BBSiOx catalysts showing the reduction of 4-NP ion to 4-AP. (For interpretation of the references to color in this figure legend, the reader is referred to the web version of this article.)

parameters.

3.3. Determination of catalytic reduction Data

After adsorption experiments, catalytic reduction experiments were carried out in batches at different temperatures with a fixed concentration (as mentioned in the experimental section) of aqueous 4-nitrophenol (4-NP), Pt-SiO_x catalyst and $NaBH_4$ solutions inside a 3.5 mL quartz cuvette. The suspensions were stirred at selected temperatures of 30, 40, 50, 60, and 70 °C, respectively. At fixed time intervals, samples were withdrawn from the reaction mixture and analyzed in a UV/vis/NIR spectrophotometer.

Table 1
Thermodynamic parameter values for the catalytic reduction of 4-NP using Pt-RHSiOx, Pt-BBSiOx and Pt-EMSiOx hybrid catalysts calculated using Gibbs free energy and Arrhenius equation calculation models.

Catalyst	T (°C)	Time (s)	TOC	K_{app} (s^{-1})	ΔG	Ea (kJ mol^{-1})	ΔH (kJ mol^{-1})	ΔS (J mol^{-1} K^{-1})
Pt-RHSiOx	30	105	1.81	0.029	83.4	26.73	22.630	−206.7
	40	90	2.10	0.031	85.5			
	50	70	2.70	0.042	87.5			
	60	50	3.79	0.057	89.6			
	70	30	6.3	0.084	91.7			
Pt-BBSiOx	30	180	1.42	0.012	87.9	15.74	12.836	−239.1
	40	150	1.7	0.016	90.4			
	50	120	2.13	0.018	92.8			
	60	100	2.57	0.023	95.2			
	70	80	3.21	0.025	97.5			
Pt-EMSiOx	30	80	1.88	0.024	94.4	31.82	29.248	−215.3
	40	60	2.5	0.037	96.5			
	50	50	3.00	0.047	98.7			
	60	30	5.00	0.072	100.8			
	70	20	7.59	0.111	102.9			

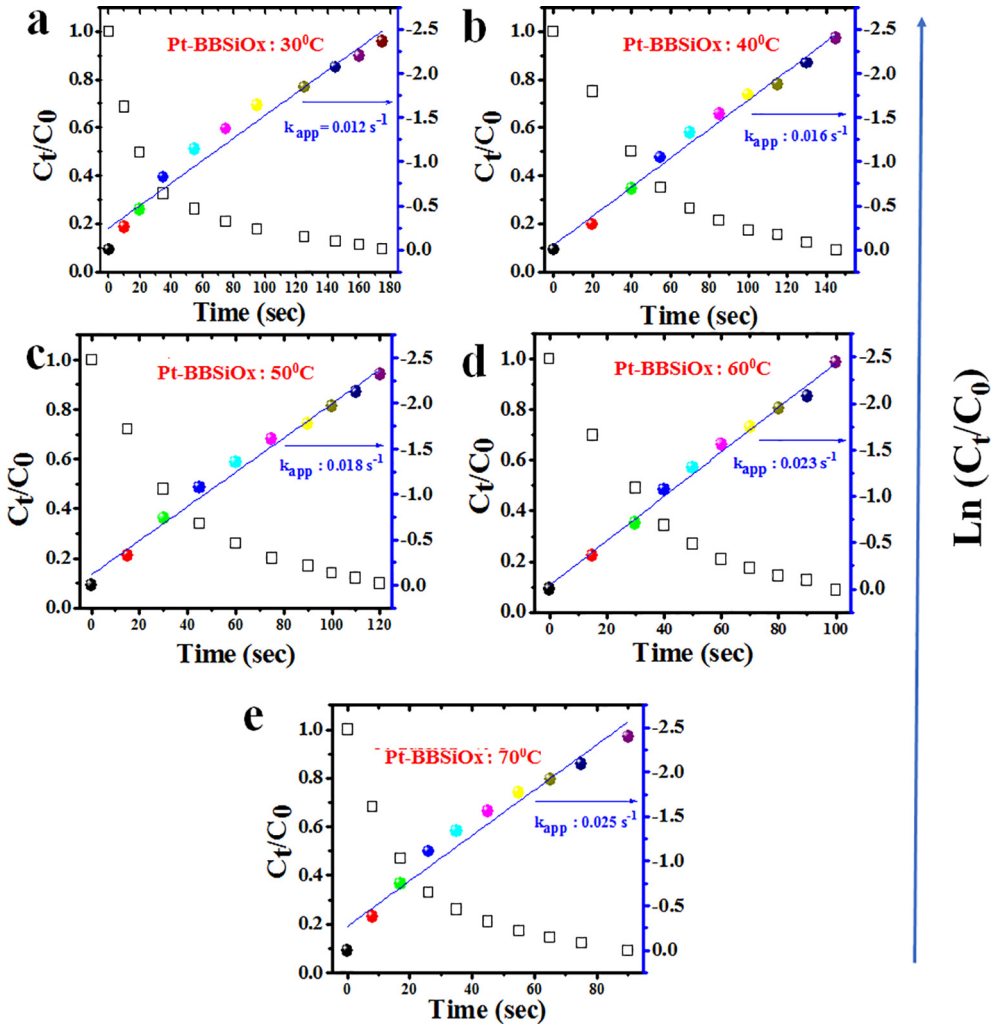

Fig. 6. Kinetics of Pt-BBSiOx catalytic reaction at (a) 30 °C, (b) 40 °C, (c) 50 °C, (d) 60 °C and (e) 70 °C. Corresponding rate constants (k_{app}) are 0.012, 0.016, 0.018, 0.023 and 0.025 s^{-1} respectively.

3.3.1. Calculation of thermodynamic parameters

The thermodynamic parameters, i.e., Gibbs free energy (ΔG), activation energy (E_a), enthalpy (ΔH) and entropy (ΔS) can be obtained from the following mathematical equations:

Gibbs free energy calculation:

$$\Delta G = \Delta H - T\Delta S \quad (1)$$

The activation energy of the adsorption process was calculated using Arrhenius equation as follows:

$$\ln(k) = \ln(A) - \frac{E_a}{RT} \quad (2)$$

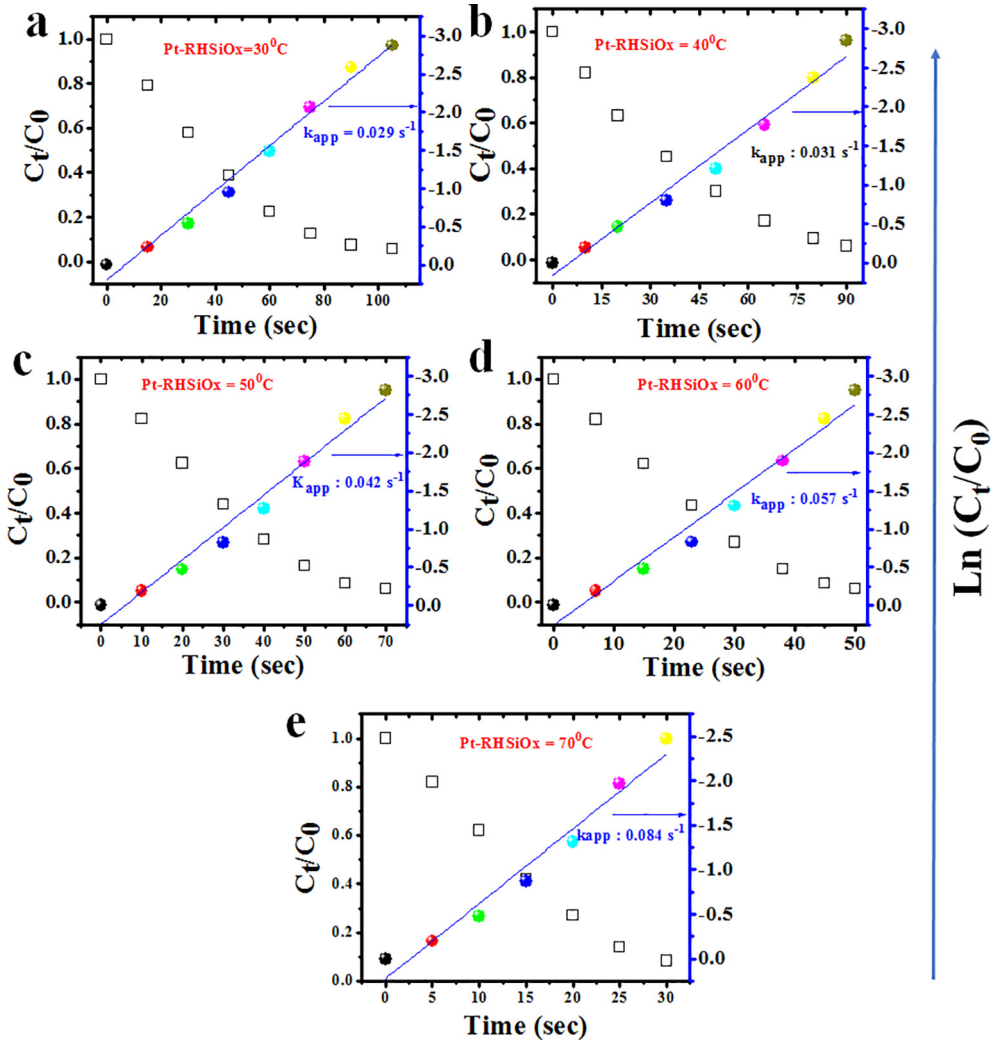

Fig. 7. Kinetics of Pt-RHSiOx catalytic reaction at (a) 30 °C (b) 40 °C (c) 50 °C (d) 60 °C and (e) 70 °C. Corresponding rate constants (k_{app}) estimated as 0.029, 0.031, 0.042, 0.057 and 0.084 s^{-1} respectively.

$$\ln(k) = -\frac{E_a}{RT} + \ln(A) \quad (3)$$

$$\ln(k) = \left(-\frac{E_a}{R}\right)\frac{1}{T} + \ln(A) \quad (4)$$

$\ln(k) \text{vs} \frac{1}{T}$

$-\frac{Ea}{R}$ = slope

R = gas constant (8.314 JK^{-1} mol^{-1})

Calculation of activation enthalpy (ΔH) and Entropy (ΔS) using Eyring equation:

$$\ln\left(\frac{k}{T}\right) = \ln\left(\frac{K_B}{h}\right) + \frac{\Delta S}{R} - \frac{\Delta H}{RT} \quad (5)$$

$$\ln\left(\frac{k}{T}\right) = \left(-\frac{\Delta H}{R}\right)\frac{1}{T} + \ln\left(\frac{K_B}{h}\right) + \frac{\Delta S}{R} \quad (6)$$

$\ln\left(\frac{k}{T}\right) \text{vs} \frac{1}{T}$

from the slope of the graph one can calculate the change in enthalpy

i. e. ,$\left(-\frac{\Delta H}{R}\right)$ = slope

and entropy from the constant (c)

$\ln\left(\frac{K_B}{h}\right) + \frac{\Delta S}{R}$ = constant(c); from the $\ln\left(\frac{k}{T}\right) \text{vs} \frac{1}{T}$ graph

- where, A = Arrhenius constant,
- R = 8.314 $J.k^{-1}.mol^{-1}$;
- K_B = 1.381*10^{-23} $J.K^{-1}$;
- h = 6.626*10^{-34} $J.k^{-1}.mol^{-1}$;
- T = absolute temperature in kelvin;
- k = k_{app} = pseudo-first-order rate constant

3.3.2. Thermodynamic properties

Thermodynamic analysis of the present catalytic reduction process was carried out by varying the reaction temperature from 30 to 70 °C with a step size of 10 °C. As can be noticed form Figs. 6–8, a total reduction of 4-nitrophenol strongly depends on the reaction temperature for all the hybrid catalysts. At higher temperatures, the reduction process (of 4-NP) is very fast (Fig. 10a) with increasing rate constants (k_{app}), compared to the reactions performed at room temperature (Fig. 10b). To obtain thermodynamic information, Gibbs free energy and activation energy of the catalytic reduction process were calculated using Arrhenius equation from the kinetics of the conversion reaction of 4-NP. For all the composite catalysts, we examined the correlation between $\ln(C_t/C_0)$ vs reaction time at all the reaction temperatures

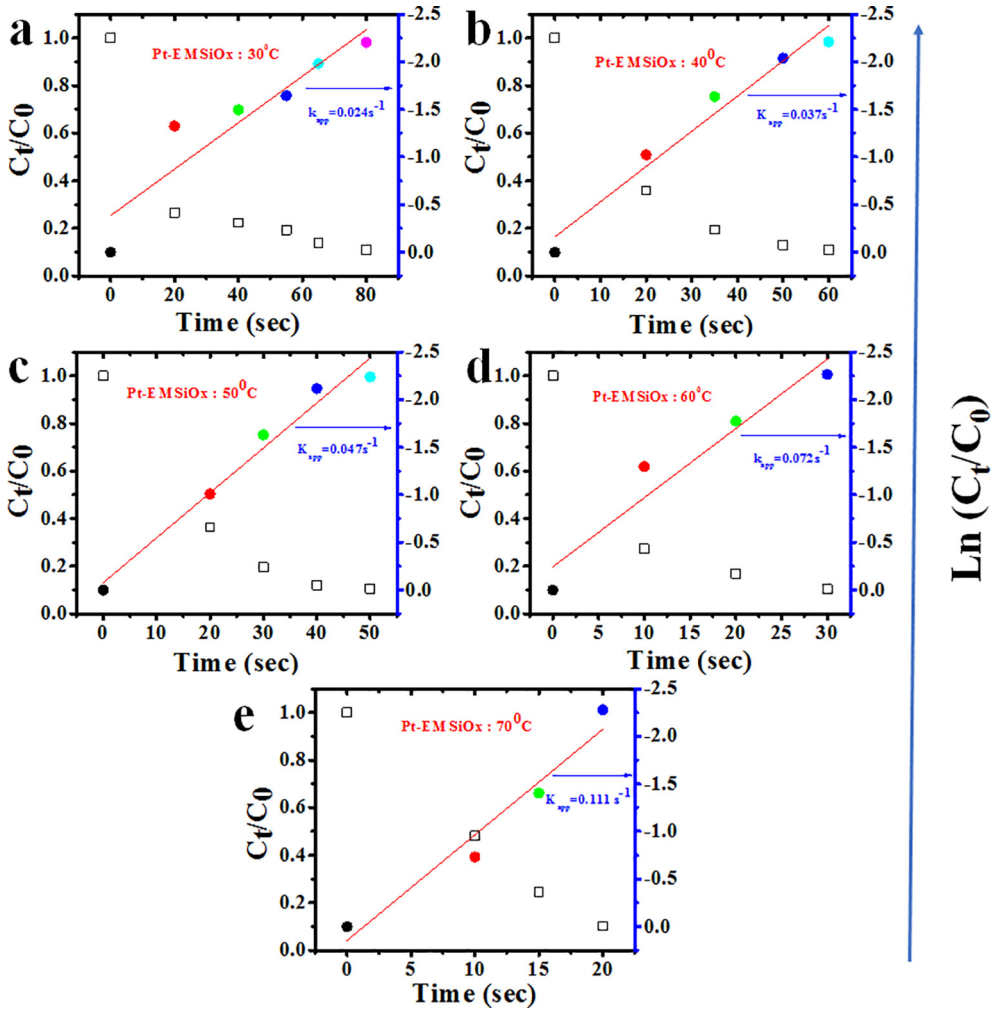

Fig. 8. Kinetics of Pt-EMSiOx catalytic reaction at different temperatures at (a) 30 °C, (b) 40 °C, (c) 50 °C, (d) 60 °C and (e) 70 °C and the corresponding rate constants (k_{app}) are 0.024, 0.037, 0.047, 0.072 and 0.111 s^{-1} respectively.

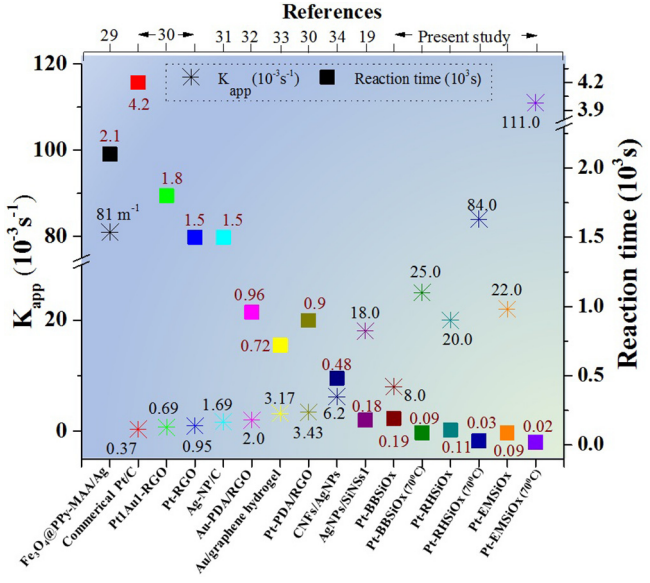

Fig. 9. Comparison of the catalytic performances of various supported Ag/Au/Pt catalysts [19,29–34].

(Figs. 6–8). The reactions were seen to follow the pseudo-first-order approximation, and the apparent rate constants k_{app} were obtained from the slope of $\ln(C_t/C_0)$ vs reaction time (Table 1 and Fig. 8). Although, an increase in rate constant was observed for all the catalysts on increasing the reaction temperature, the value of "k_{app}" was highest (1.11×10^{-3} s^{-1}) for the catalyst Pt-EMSiOx and 70 °C reaction temperature. Estimated "k_{app}" values for the Pt-RHSiOx and Pt-BBSiOx catalysts at the same reaction temperature were 8.4×10^{-2} s^{-1}, and 2.5×10^{-2} s^{-1}, respectively.

The thermodynamic parameters of the system, i.e., Gibbs free energy (ΔG), activation energy (E_a), enthalpy (ΔH) and entropy (ΔS) estimated using Fig. 10(c–e)) are presented in Table 1. The ΔG values for all the hybrid catalysts were positive, revealing an endergonic process with higher ΔG (102.9 k.J.mol^{-1}) in case of EMSiOx (at 70 °C) as compared with RHSiOx and BBSiOx silica substrates with ΔG values of 91.7 and 97.5 kJ mol^{-1}, respectively. The activation energy (E_a) estimated for the BB, RHs and EM SiOx supported Pt catalysts were 15.74, 26.73 and 31.82 kJ mol^{-1}, respectively.

The relation between the enthalpy and the catalytic reduction capacity of the hybrid catalysts can be considered as the interaction energy of molecules adsorbed at the adsorbent-adsorbate interface [34–36]. Estimated enthalpy (ΔH) values are positive for all the catalysts, showing the endothermic nature of the catalytic reduction process, with maximum catalytic reduction of 4-NP for the Pt-EMSiOx catalyst (EM silica substrate) (ΔH = 29.248 kJ mol^{-1}), and minimum (ΔH = 12.836 kJ mol^{-1}) for BBSiOx.

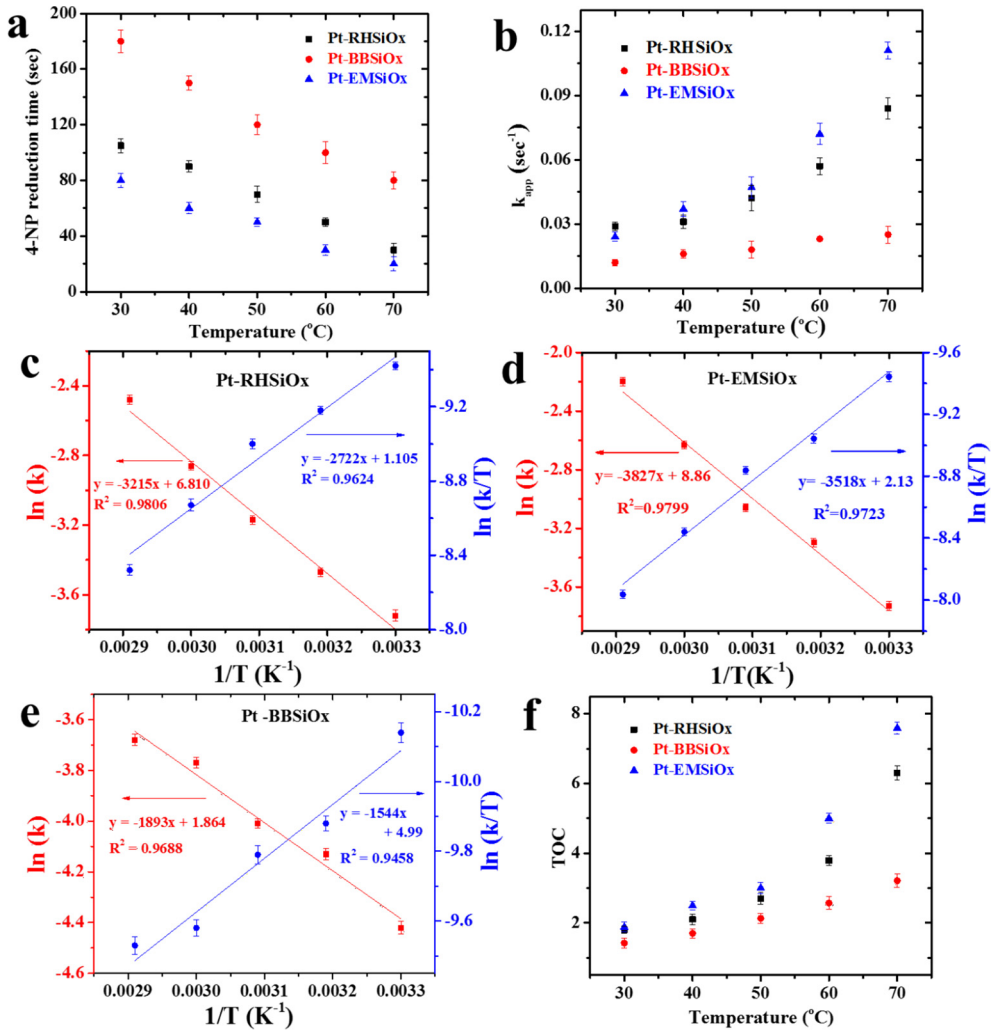

Fig. 10. Kinetics of (a) temperature dependent reduction of 4-NP, and (b) rate constants vs temperature (calculated from the plots ln (C_t/C_0) corresponding to the reduction of 4-NP with time studied as a function of temperature). The thermodynamic parameters such as activation energy, enthalpy and entropy were calculated (details given in Table 1) using plots ln (k) vs 1/T (K^{-1}) and ln (k/T) vs 1/T (K^{-1}) for (c) Pt-RHSiO$_x$, (d) Pt-EMSiO$_x$, (e) Pt-BBSiO$_x$ and (f) Turn over capacity (TOC) of the hybrid catalysts.

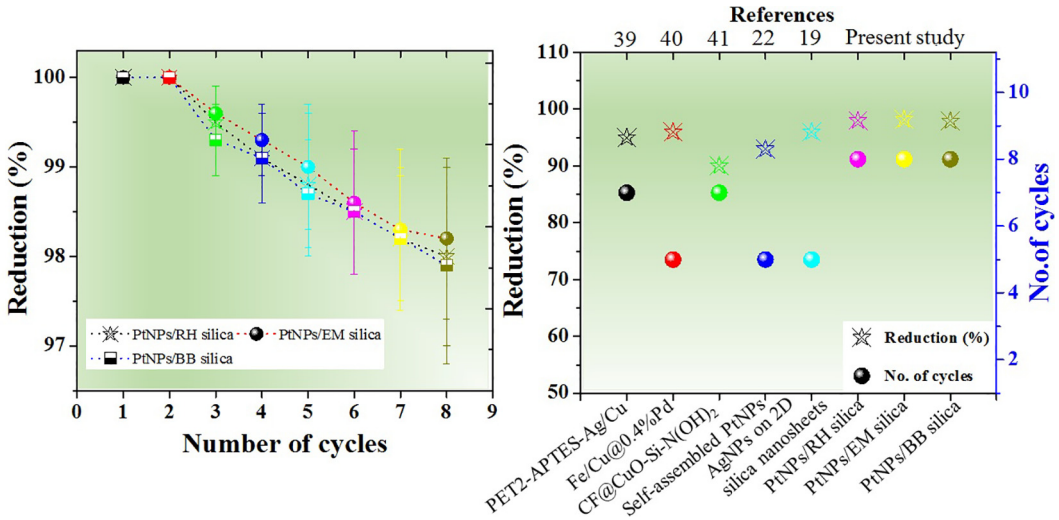

Fig. 11. (a) Re-usability of 3D biogenic silica (RHSiOx, black), EMSiOx (red) and BBSiOx (blue)) supported PtNPs and (b) Comparison of the reusability performance of the tested hybrid catalysts with the similar catalysts reported in the literature [19,22,39–41]. (For interpretation of the references to color in this figure legend, the reader is referred to the web version of this article.)

The change in entropy (ΔS) of our systems has also been estimated due to their direct relation with the association of the adsorbate at the solid-solution interface. A negative value of ΔS suggests that the disorder of the system decreases with the reduction in the number of reactant molecules. As the changes in ΔS values are linked to the movement of molecules adsorbed by the adsorbate, the value (-206.7 J mol^{-1} K^{-1}) corresponding to PtNPs/RHs silica substrate was found to be low. Therefore, it can be inferred that more water molecules are displaced by phenol derivatives with higher substitution degrees on the surface of these silica substrates.

3.3.3. Turnover capacity (TOC)

The turnover capacity (TOC) is one important parameter to evaluate the catalytic performance of PtNPs, which can be calculated by dividing the molar mass of the 4-NP with the molar mass of the PtNPs and reaction time (Table 1). As the size and shape of the NPs contribute significantly on the catalytic performance [37,38] of the nanomaterials due to change in surface-to-volume ratio and size-dependent redox potential, which, in turn, can promote the interfacial electron transfer from the surface of the PtNPs to 4-NP in the presence of high concentration of electron injecting BH_4^- ions. Hence, much higher TOC value of the PtNPs supported over EMSiOx substrate at 70 °C (7.59 min^{-1}) with respect to the other two composite catalysts RHSiOx and BBSiOx (6.3 and 3.21 min^{-1}) is attributed to the presence of relatively higher number of PtNPs over it (Fig. 10f), which causes a faster interfacial electron transfer from PtNPs surface to 4-NP. Additionally, in conformity with the EDS, TEM and XPS results, the EMSiOx supported catalyst contains higher Pt wt.% compared to other substrates, resulting in its higher catalytic performance.

Considering the average particle size of ≈2.2 nm of the PtNPs (from HR-TEM analysis) and contents (from XPS analysis) of Pt in the Pt-EMSiOx, Pt-RHSiOx, and Pt-BBSiOx hybrid catalysts (0.82, 0.65 and 0.48 wt%, respectively), the excellent catalytic activity of the Pt-EMSiOx catalyst can be attributed to the high density of small, well-dispersed PtNPs at its surface, which offers higher number of active sites for effective contact with the reactant molecules and fast interfacial electron transfer from PtNPs to 4-NP. Moreover, as can be seen in Fig. 11, the proposed hybrid catalysts offer high reusability for the reduction of 4-NP with $NaBH_4$ as compared the already reported catalysts [19,22,39–41]. Even after 8 cycles, the catalytic activity of the catalysts remains almost unchanged (only about 3% decrease), which confirms the high stability of 3D silica substrates for catalytic applications. The decrease in 4-NP to 4-AP conversion efficiency with each reaction cycle can be attributed to the loss of Pt NPs from the catalyst support during recycling. XRD studies were carried out over the used catalysts to identify the change (if any) in crystallinity or structural phase after their repeated use (Fig. 12). As can be noticed in Fig. 12, the diffraction bands in the spectra of the used (in 4-NP reduction) catalyst are less intense and broader than corresponding diffraction bands of unused or fresh catalysts (Fig. 2), indicating a loss of crystallinity or decrease in amount of PtNPs on the catalyst supports. While a decrease of PtNPs from the hybrid catalysts is expected to reduce their catalytic performance in 4-NP reduction, the recycling tests performed over them revealed only a marginal reduction in their performance.

In order to mimic the purification of real polluted water (contaminated by 4-NP), an additional experimental device for “filtering and catalyzing” (under partial vacuum) was set up using the procedure reported in the literature [30] (Fig. S4; SI). The concentration and amount of 4-NP, catalyst, and $NaBH_4$ for this experiment were similar to that considered for the first reduction cycle for each of the catalysts. As a result, within 10 s (details given in Fig. S4 (b)) the visual change in the appearance of the filtered water from bright yellow (visual) to light yellow (Fig. S4b, SI) confirmed the (almost) instantaneous formation of 4-nitrophenolate ion. Furthermore, after another 20 s (Fig. S4c, SI), the colorless water, the disappearance of UV–vis absorption band associated to 4-NP at around 400 nm and the appearance of new peak around 300 nm (due to the formation of 4-AP) confirmed the complete reduction of 4-NP (Fig. S4d, SI). The result clearly indicates that the fabricated hybrid catalyst (especially the Pt-EMSiOx catalyst), can be utilized for fast and efficient reduction purification of 4-NP-contaminated waste water.

In order to make the process economically more viable and scalable, reusability of the Pt salt was also tested for 3 successive cycles. Corresponding XRD is given in Fig. S5 supported by Table S1.

3.3.4. Proposed mechanism for the conversion of 4-NP to 4-AP using Pt-SiOx as catalyst

The reactions involved in the catalytic reduction of 4-nitrophenol to 4-aminophenol by Pt decorated biogenic porous silica are shown in schematic 2. In the initial phase, the excessive amount of borohydride BH_4^{-1} ions (from $NaBH_4$) get adsorbed on the surface of Pt nanoparticles, promote the formation of Pt-hydride bonds. Consequently, adsorption of 4-nitrophenolate ion onto the Pt nanoparticles is followed by the interaction of nitro group (from 4-nitrophenolate ion) with the hydride ions to form Pt-hydride complex. Eventually, 4-aminophenol is formed as the final product through different steps of hydro-deoxygenation reactions. The Pt NPs present on the porous walls of biogenic silica substrates enhance the rate of reaction by increasing the flow of electrons from BH_4^{-1} to 4-NP [42]. The outstanding catalytic activity of Pt-SiOx for the conversion of 4-NP to 4-AP is probably due to strong synergetic effect (i.e. geometric and electron effect) between SiOx and Pt. The biogenic porous silica particles can assist the electron relay and hence improve the catalytic activity of the Pt in Pt-SiOx catalyst for the reduction 4-NP. The difference in the catalytic performance of the three types of hybrid catalysts tested in the present work is attributed not only to the different weight percent of Pt incorporated onto the porous substrates but also to the formation of uniformly distributed Pt nanoparticles (which is the case of Pt-EM SiOx). In other words, relatively higher porosity of the Pt-EMSiOx hybrid catalyst leads to the generation of higher number of catalytically active sites (small sized Pt nanoparticles) for the catalytic reduction of 4-NP. Therefore, the presence of

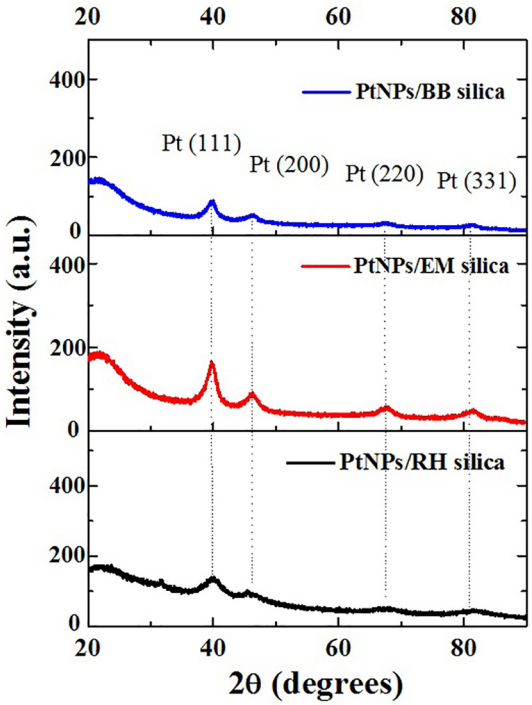

Fig. 12. XRD patterns of the hybrid catalysts (Pt-incorporated biogenic BB, EM, and RH silica substrates) after their use in 8 catalysis cycles. As compared to Pt peaks from unused catalysts (Fig. 2), the relative change in the Si/Pt peak intensities reveals the decrease in the Pt content.

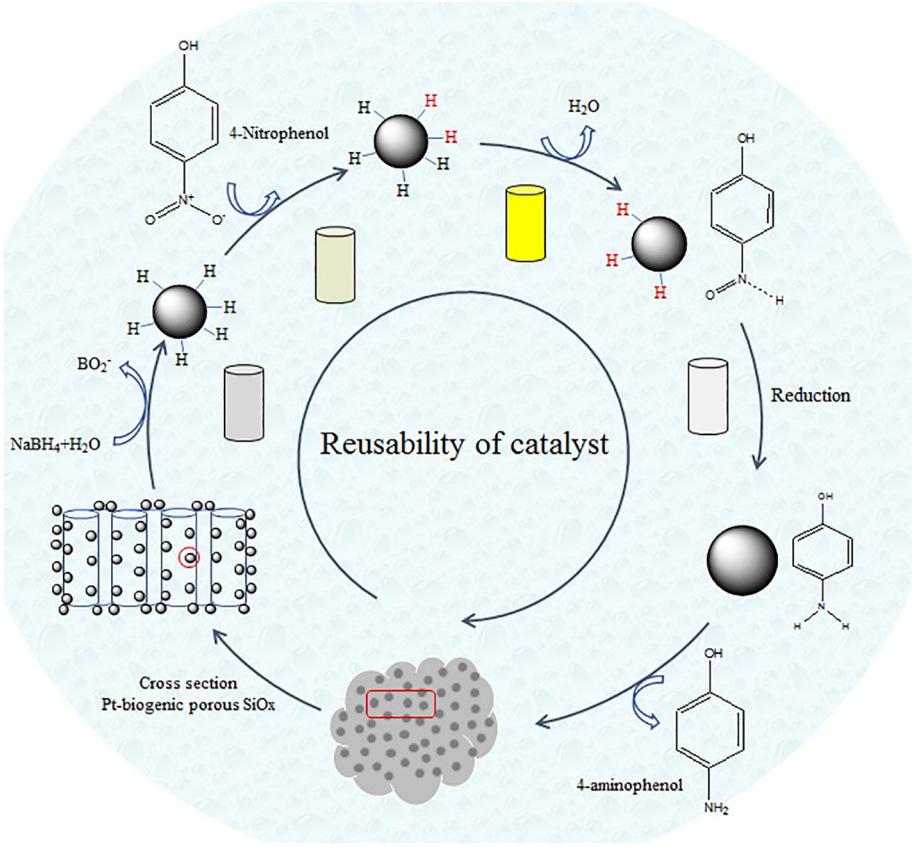

Scheme 2. Schematic representation of the mechanistic aspects of catalytic reduction reaction process for the conversion of 4-nitrophenol to 4-aminophenol in presence of $NaBH_4$ and PtNPs over mesoporous 3D biogenic silica substrates. (H in red represents the participation in the next step in the reaction).

biogenic porous silica substrates in Pt-SiOx plays a vital role in enhancing the catalytic reduction process. Additionally, the highly porous biogenic silica (ref to Fig. 4c) can also act as in-built depth filter to trap part of the suspended contaminants (smaller than the pore volume) within the depth of the porous catalytic system.

4. Conclusions

In our pursuit for obtaining reusable efficient environment friendly catalyst, small Pt nanoparticles of 2 to 3 nm (mean size = 2.2 nm) sizes could be successfully fabricated and assembled over the surface of 3D porous biogenic silica substrates of different biological origins through a simple two-step chemical process. The size and density of Pt nanoparticles over different biogenic silica supports is found to depend on substrate porosity and surface coverage by amino groups (from APTES) at their surface. All the fabricated hybrid structures show high catalytic activity for 4-NP reduction by $NaBH_4$, with a complete reduction as fast as in 90 s at room temperature and within 20 s at 70 °C. The best catalytic performance manifested by the Pt-EMSiOx catalyst could be associated to the higher surface area (high porosity) of EM silica and good dispersion of Pt nanoparticles over it. While a good dispersion and high density of Pt particles generate a high density of active catalytic sites at the surface of the catalyst, high porosity of the support not only facilitates a good adsorption of analyte molecules at surface, but also enhances the electron transfer process from Pt nanoparticles to the analyte (4-NP) molecules. The hybrid catalysts fabricated in this work are highly stable (chemical and thermal), have good reusability (up to 8 cycles with less than 3% reduction) performance, and can be efficiently utilized for fast purification of 4-NP contaminated waste water. The hybrid PtNPs supported biogenic silica catalysts have great potential for commercialization after optimization of PtNP loading over the porous substrates.

Declaration of Competing Interest

The authors declare that they have no known competing financial interests or personal relationships that could have appeared to influence the work reported in this paper.

Acknowledgements

VA acknowledges the support from CONACyT (Infrastructure project 2014: 226291) for acquiring the field emission scanning electron microscope. Additionally, we acknowledge biogenic silica from Concretio silicea bambuseae (Bamboo), provided by Dr. L.T. Canham. We acknowledge the useful discussions with Dr. Hernan Larralde Ridaura (Instituto de Ciencias Fisicas -UNAM). Technical help from Mary Cruz Resendiz (SEM) and Jose Juan Ramos Hernandez (XRD) is acknowledged. NKRB and PS contributed equally.

Appendix A. Supplementary data

Supplementary data to this article can be found online at https://doi.org/10.1016/j.cej.2020.124237.

References

[1] V. Janout, S.B. Myers, R.A. Register, S.L. Regen, Self-cleaning resins, J. Am. Chem. Soc. 129 (2007) 5756–5759, https://doi.org/10.1021/ja068679f.
[2] T. Ono, T. Sugimoto, S. Shinkai, K. Sada, Lipophilic polyelectrolyte gels as superabsorbent polymers for nonpolar organic solvents, Nat. Mater. 6 (2007) 429–433, https://doi.org/10.1038/nmat1904.
[3] Y. Chu, Q. Pan, Three-dimensionally macroporous Fe/C nanocomposites as highly selective oil-absorption materials, ACS Appl. Mater. Inter. 4 (2012) 2420–2425, https://doi.org/10.1021/am3000825.
[4] M. Inagaki, A. Kawahara, H. Konno, Sorption and recovery of heavy oils using carbonized fir fibers and recycling, Carbon 40 (2002) 105–111, https://doi.org/10.

1016/S0008-6223(01)00083-5.
[5] J. Yuan, X. Liu, O. Akbulut, J. Hu, S.L. Sui, J. Kong, F. Stellacci, Superwetting nanowire membranes for selective absorption, Nat. Nanotechnol. 3 (2008) 332–336, https://doi.org/10.1038/nnano.2008.136.
[6] C. Wu, X. Huang, X. Wu, R. Qian, P. Jiang, Mechanically flexible and multifunctional polymer-based graphene foams for elastic conductors and oil-water separators, Adv. Mater. 25 (2013) 5658–5662, https://doi.org/10.1002/adma.201302406.
[7] A. Sayari, S. Hamoudi, Y. Yang, Applications of pore-expanded mesoporous silica. 1. Removal of heavy metal cations and organic pollutants from wastewater, Chem. Mater. 17 (2005) 212–216, https://doi.org/10.1021/cm048393e.
[8] H. Bi, X. Xie, K. Yin, Y. Zhou, S. Wan, L. He, F. Xu, F. Banhart, L. Sun, R.S. Ruoff, Spongy graphene as a highly efficient and recyclable sorbent for oils and organic solvents, Adv. Funct. Mater. 22 (2012) 4421–4425, https://doi.org/10.1002/adfm.201200888.
[9] R.R. Arvizo, S. Bhattacharyya, R.A. Kudgus, K. Giri, R. Bhattacharya, P. Mukherjee, Intrinsic therapeutic applications of noble metal nanoparticles: past, present and future, Chem. Soc. Rev. 41 (2012) 2943–2970, https://doi.org/10.1039/C2CS15355F.
[10] Z. Zhang, Y. Huang, K. Liu, L. Guo, Q. Yuan, B. Dong, Multichannel-improved charge-carrier dynamics in well-designed hetero-nanostructural plasmonic photocatalysts toward highly efficient solar-to-fuels conversion, Adv. Mater. 27 (2015) 5906–5914, https://doi.org/10.1002/adma.201502203.
[11] B.K. Min, C.M. Friend, Heterogeneous gold-based catalysis for green chemistry: low-temperature CO oxidation and propene oxidation, Chem. Rev. 107 (2007) 2709–2724, https://doi.org/10.1021/cr050954d.
[12] C.W. Corti, R.J. Holliday, D.T. Thompson, Commercial aspects of gold catalysis, Appl. Catal. A: Gen. 291 (2005) 253–261, https://doi.org/10.1016/j.apcata.2005.01.051.
[13] D. Astruc, F. Lu, J.R. Aranzaes, Nanoparticles as recyclable catalysts: the frontier between homogeneous and heterogeneous catalysis, Angew. Chem. Int. Ed. 44 (2005) 7852–7872, https://doi.org/10.1002/anie.200500766.
[14] Y. Li, Y.L. Jeremy, L. Jingjing, Y. Jingfang, L. Zhiping, W. Weixing, S. Luyi, Synthesis of gold nanoparticles on rice husk silica for catalysis applications, Ind. Eng. Eng. Res. 54 (2015) 5656–5663, https://doi.org/10.1021/acs.iecr.5b00216.
[15] B. Yu, J. Xu, J.-H. Liu, S.-T. Yang, J. Luo, Q. Zhou, J. Wan, R. Liao, H. Wang, Y. Liu, Adsorption behavior of copper ions on graphene oxide–chitosan aerogel, J. Environ. Chem. Eng. 1 (2013) 1044–1050, https://doi.org/10.1016/j.jece.2013.08.017.
[16] G. Eichenbaum, M. Johnson, D. Kirkland, P. O'Neill, S. Stellar, J. Bielawne, R. DeWire, D. Areia, S. Bryant, S. Weiner, D. Desai-Krieger, P. Guzzie-Peck, D.C. Evans, A. Tonelli, Assessment of the genotoxic and carcinogenic risks of *p*-nitrophenol when it is present as an impurity in a drug product, Regul. Toxicol. Pharmacol. 55 (2009) 33–42, https://doi.org/10.1016/j.yrtph.2009.05.018.
[17] N.K.R. Bogireddy, R.C. Silva, A.V. Miguel, V. Agarwal, 4-nitrophenol optical sensing with N doped oxidized carbon dots, J. Haz. Mat. 386 (2020) 121643, https://doi.org/10.1016/j.jhazmat.2019.121643.
[18] J. Ma, X. Guo, Y. Zhang, H. Ge, Catalytic performance of TiO2@ Ag composites prepared by modified photodeposition method, Chem. Eng. J. 258 (2014) 247–253, https://doi.org/10.1016/j.cej.2014.06.120.
[19] Z. Yan, L. Fu, X. Zuo, H. Yang, Green assembly of stable and uniform silver nanoparticles on 2D silica nanosheets for catalytic reduction of 4-nitrophenol, Appl. Cat. B: Environ. 226 (2018) 23–30, https://doi.org/10.1016/j.apcatb.2017.12.040.
[20] J. Li, F. Wu, L. Lin, Y. Guo, H. Liu, X. Zhang, Flow fabrication of a highly efficient Pd/UiO-66-NH_2 film capillary microreactor for 4-nitrophenol reduction, Chem. Eng. J. 333 (2018) 146–152, https://doi.org/10.1016/j.cej.2017.09.154.
[21] S.R. Anna, S. Padma, J.H. Graham, V. Marco, T.C. Leigh, C.P. Carole, A. Vivechana, Biogenic porous silica and silicon sourced from Mexican Giant Horsetail (Equisetum myriochaetum) and their application as supports for enzyme immobilization, Col. Surf B: Biointer. 166 (2018) 195–202, https://doi.org/10.1016/j.colsurfb.2018.02.047.
[22] N.K.R. Bogireddy, L.M. Gomez, I.O. Roman, V. Agarwal, Synthesis of gold nanoparticles using *coffea arabica* fruit extract, Adv. Nano Res. 5 (2017) 253–260, https://doi.org/10.12989/anr.2017.5.3.253.
[23] K.M. In, L. Junghyun, S.R. Rodney, L. Hyoyoung, Reduced graphene oxide by chemical graphitization, Nature Comm. 1 (2010) 73, https://doi.org/10.1038/ncomms1067.
[24] G. Hollinger, Y. Jugnet, P. Pertosa, T.M. Duc, X-ray photoelectron spectroscopy of thermally grown silicon dioxide films on silicon, Chem. Phys. Lett. 36 (1975) 441–445, https://doi.org/10.1016/0009-2614(75)80276-4.
[25] G.F. Cerofolini, C. Galati, L. Renna, Si 2p XPS spectrum of the hydrogen-terminated (100) surface of device-quality silicon, Surf. Interface Anal. 35 (2003) 968–973, https://doi.org/10.1002/sia.1632.
[26] C.H.F. Peden, J.W. Rogers, N.D. Shinn Jr., K.B. Kidd, K.L. Tsang, Thermally grown Si3N4 thin films on Si(100): surface and interfacial composition, Phys. Rev. B 47 (1993) 15622–15629, https://doi.org/10.1103/PhysRevB.47.15622.
[27] C.D. Wagner, W.M. Riggs, L.E. Devis, J.F. Moulder, G.E. Muilenberg (Eds.), Handbook of X-ray photoelectron spectroscopy, Perkin-Elmer Corporation, Minnesota, 1979.
[28] B. Baruah, G.J. Gabriel, M.J. Akbashev, M.E. Booher, Facile synthesis of silver nanoparticles stabilized by cationic polynorbornenes and their catalytic activity in 4-nitrophenol reduction, Langmuir 29 (2013) 4225–4234, https://doi.org/10.1021/la305068p.
[29] R. Das, V.S. Sypu, H.K. Paumo, M. Bhaumik, V. Maharaj, A. Maity, Silver decorated magnetic nanocomposite (Fe3O4@PPy-MAA/Ag) as highly active catalyst towards reduction of 4-nitrophenol and toxic organic dyes, App. Cat. B: Environ. 244 (2019) 546–558, https://doi.org/10.1016/j.apcatb.2018.11.073.
[30] W. Ye, J. Yu, Y. Zhou, D. Gao, D. Wang, C. Wang, D. Xue, Green synthesis of Pt–Au dendrimer-like nanoparticles supported on polydopamine-functionalized graphene and their high performance toward 4-nitrophenol reduction, Appl. Cat. B: Environ. 182 (2016) 371–378, https://doi.org/10.1016/j.apcatb.2015.08.013.4.
[31] W. Ye, J. Yu, Y. Zhou, D. Gao, D. Wang, C. Wang, D. Xue, Green synthesis of Pt–Au dendrimer-like nanoparticles supported on polydopamine-functionalized graphene and their high performance toward 4- nitrophenol reduction, Appl. Catal. B: Environ. 181 (2016) 371–378, https://doi.org/10.1016/j.apcatb.2015.08.013.
[32] S. Tang, S. Vongehr, X. Meng, Carbon spheres with controllable silver nanoparticle doping, J. Phys. Chem. C 114 (2010) 977–982, https://doi.org/10.1021/jp9102492.
[33] J. Li, C. Liu, Y. Liu, Au/graphene hydrogel: synthesis, characterization and its use for catalytic reduction of 4-nitrophenol, J. Mater. Chem. 22 (2012) 8426–8430, https://doi.org/10.1039/C2JM16386A.
[34] P. Zhang, C. Shao, Z. Zhang, M. Zhang, J. Mu, Z. Guo, Y. Liu, In situ assembly of well-dispersed Ag nanoparticles (AgNPs) on electrospun carbon nanofibers (CNFs) for catalytic reduction of 4-nitrophenol, Nanoscale 3 (2011) 3357–3363, https://doi.org/10.1039/C1NR10405E.
[35] P.J. Dauenhauer, O.A. Abdelrahman, A universal descriptor for the entropy of adsorbed molecules in confined spaces, ACS Cent. Sci. 4 (2018) 1235–1243, https://doi.org/10.1021/centsci.8b00419.
[36] C.T. Campbell, J.R.V. Sellers, The entropies of adsorbed molecules, J. Am. Chem. Soc. 134 (2012) 18109–18115, https://doi.org/10.1021/ja3080117.
[37] M. Kamali, T. Gameiro, M.E. Costa, I. Capela, T.M. Aminabhavi, Enhanced biodegradation of phenolic wastewaters with acclimatized activated sludge – a kinetic study, Chem. Eng. J. 378 (2019) 122186, , https://doi.org/10.1016/j.cej.2019.122186.
[38] M. Kamali, M.E. Costa, T.M. Aminabhavi, I. Capel, Sustainability of treatment technologies for industrial biowastes effluents, Chem. Eng. J. 370 (2019) 1511–1521, https://doi.org/10.1016/j.cej.2019.04.010.
[39] B. Nabil, N.M. Mohammad, E.A. Ahmida, N. Behary, C. Christine, V. Julien, O. Thoumire, A. Abdelkrim, Development of new multifunctional filter based nonwovens for organics pollutants reduction and detoxification: high catalytic and antibacterial activities, Chem. Eng. J. 356 (2019) 702–716, https://doi.org/10.1016/j.cej.2018.08.166.
[40] C. Xu, X. Pan, L. Fang, J. Li, F. Li, Enhanced reduction of organic pollutants by Fe/Cu@Pd ternary metallic nanoparticles under aerobic conditions: Batch and membrane reactor studies, Chem. Eng. J. 360 (2019) 180–189, https://doi.org/10.1016/j.cej.2018.11.212.
[41] B. Nabil, E.A. Ahmida, C. Christine, V. Julien, A. Abdelkrim, Polyfunctional cotton fabrics with catalytic activity and antibacterial capacity, Chem. Eng. J. 351 (2018) 328–339, https://doi.org/10.1016/j.cej.2018.06.050.
[42] N.K.R. Bogireddy, U. Pal, L.M. Gomez, V. Agarwal, Size controlled green synthesis of gold nanoparticles using Coffea Arabica seed extract and their catalytic performance in 4-nitrophenol reduction, RSC Adv. 8 (2018) 24819–24856, https://doi.org/10.1039/C8RA04332A.